2003

JETS AND SPRAYS EMITTED FROM COLLOID THRUSTERS - EXPERIMENTS AND MODELING

Paulo Lozano* and Manuel Martinez-Sanchez**

Massachusetts Institute of Technology, Dept. of Aeronautics and Astronautics
77 Massachusetts Avenue, Cambridge, MA 02139 USA
*Doctoral Candidate. Room 37-438/Phone: 617-253-7485/Email: plozano@mit.edu
**Professor. Room 37-341/ Phone: 617-253-5613/Fax: 617-258-5940/Email: mmart@mit.edu

Abstract

The spreading angle of an electrospray of Formamide with 5-10% LiCl by mass has been measured to be 18° in vacuum, for conditions close to minimum stable flow. A single-stage einzel lens was able to re-focus the spray, as predicted by paraxial ray theory. In addition, a time-dependent 1-D numerical model of the cone-jet-spray structure is described, and initial results presented.

1. Introduction

Colloid thrusters, working on the principle of electrostatic extraction and acceleration of highly charged liquid droplets, are one of several microthruster technologies currently receiving attention for applications ranging from main propulsion of microsatellites to high-precision altitude control and station keeping of constellation members. An introduction to the technology and a review of its earlier implementation as a mainline propulsion concept (in the 1960's and1970's) can be found in Ref. [1].

At MIT, we are currently pursuing several lines of research on these thrusters. In this paper we report on our progress in the direction of a better understanding and control of the spray generated by a single un-neutralized colloid emitter. One eventual goal is the construction and verification of models for evaluating the possible interactions of these propulsive beams with the spacecraft. In addition, we aim at the construction of an improved Time-of-Flight mass spectrometer for the detailed study of mixed ion-droplet sprays, which may play a prominent role in actual high-performance colloid thrusters [1]. In order to increase the resolution of this device, ion optical concepts are needed for re-focusing of the spray after its space-charge induced initial divergence.

Section 2 of this paper describes our experimental work and presents some data on beam spreading and refocusing using a custom-designed einzel lens. Section 3 describes our on-going work on numerical modeling of the colloid emitter, starting with the Taylor cone and following through to the spreading electrospray. Only preliminary results are at present available, and some of these will be discussed.

2.1 Experimental Apparatus

The main experimental goal was to measure the amount of spreading in a typical colloid jet and to determine if the charged droplets can be focused by means of external electrostatic fields.

The colloid emitter consisted of a single quartz needle with ID of 75μm and final tip ID of 30μm. Fig 1 shows a diagram of the system. Not shown is the syringe pump which was used to inject and monitor the liquid flow rate (Formamide with 5-10%wt. concentration of LiCl) into the emitter. Capacitive effects in the transfer line, however, did not allow a precise determination of the flow rate. Nevertheless we know that its value was centered, within a certain margin, at around 2×10^{-12} m^3/s.

The emitter is coated with a metallic film that allows electric contact between the liquid and a high voltage power supply (V_E). The emitter tip was positioned at the center of a circular aperture of 6 mm in diameter that served as the grounded extractor electrode. The electrostatic lens was positioned next to the extractor and was biased negatively with respect to it (V_F) by using a second high voltage power supply.

The current collector (Fig. 2) is comprised of a series of 11 concentric metallic rings, each with a width of 3mm (except the first one which is a circle with diameter of 1cm) and a maximum radius of 3.5 cm. Each ring is electrically isolated from the rest and allows one to measure current at different radii with a resolution given by the number of rings. A sensitive amperimeter was used to pick-up the signal from each ring.

Experiments were performed inside a large vacuum chamber equipped with a set of two cryogenic pumps at pressures below 1×10^{-6} torr.

2.2 Beam Spreading and Lens Design

One of the most useful techniques to characterize the beam of an electrospray is by the use of Time-of-Flight

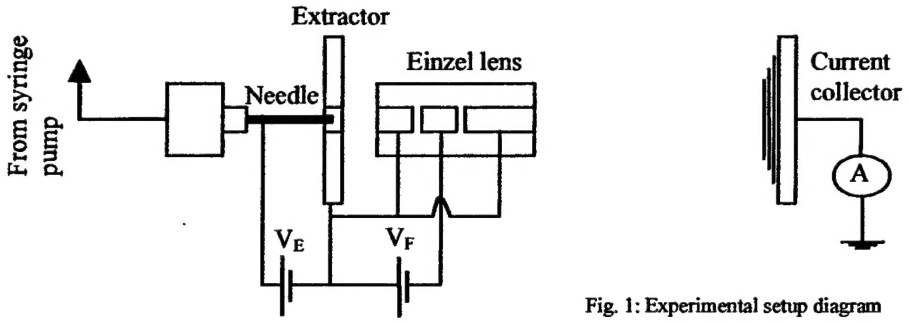

Fig. 1: Experimental setup diagram

(TOF) spectroscopy in which a beam of emitted particles is forced to drift towards an electrometer as the extractor voltage is suddenly cut. This allows one to measure the time it takes the jet to reach the target and gives therefore enough information to estimate the specific charge of the different particles that compose the beam. Specific charge and beam composition are very important to determine the performance of a thruster as the propulsive efficiency and the specific impulse depend directly on those parameters.

Since the beam is formed by charged particles, one can expect it to spread under electrostatic repulsion forces. The amount of this spreading will depend on the beam composition and its dynamic characteristics. From previous experiences [2,4], it is known that spreading limits the working distance for TOF to 20-30 cm. To solve this problem one could make use of the well developed theory of ion optics which has been applied for many years to microfabrication with liquid metal ion sources [3]. In particular, one could make use of a focusing device called "einzel" or equipotential lens. In a lens of this type, an accelerating potential is generated in the path of the charged beam, followed by a decelerating potential which leaves the particles with the same axial kinetic energy they had before entering the device, but provides a net focusing effect in the radial direction.

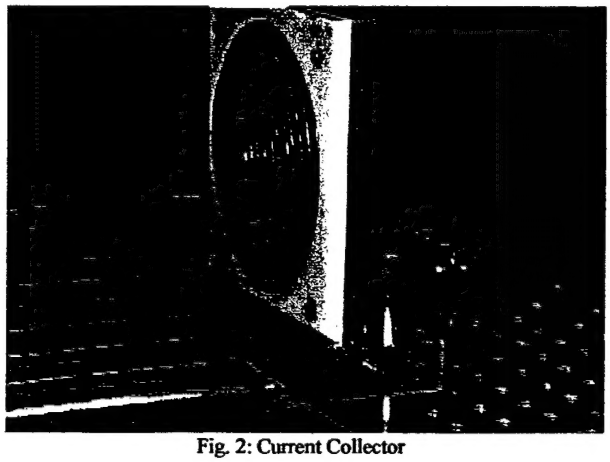

Fig. 2: Current Collector

To calculate the beam trajectory the paraxial ray equation is used. In the paraxial approximation it is assumed that the beam particles stay relatively close to the base trajectory (beam axis) and that the beam profile has a uniform charge distribution. The force equations can be solved considering axially symmetric electrostatic fields with cylindrical geometry. These fields are expressed as the first order terms of the solution in series of Poisson's equation. What is most interesting about the paraxial approximation is that we only require knowledge of the electrostatic potential (V_o) at the axis of symmetry. The paraxial ray equation can then be written as

$$r'' + \frac{V_o' r'}{2V_o} + \frac{V_o'' r}{4V_o} = -\frac{\rho_o r}{4\varepsilon_o V_o} \qquad (1)$$

where the space charge density ρ_o is given for N species in the beam as

$$\rho_o = \frac{1}{\pi r^2 \sqrt{2V_o}} \sum_{i=1}^{N} \frac{I_i}{(q/m)_i} \qquad (2)$$

I_i and $(q/m)_i$ are the current and the charge to mass ratio of the ith species in the beam. (A single species was assumed in this paper). The on-axis potential can be extracted after solving Laplace's equation for a given geometry of electrodes with the help of an elliptic solver.

Fig. 3 shows the geometry of the emitter, extractor and the lens, superimposed to the mesh used to solve Laplace's equation, and the solution itself. It is clear how the strong negative potential in the middle region of the lens is effectively shielded out by the grounded electrodes positioned in the inlet and outlet planes. The next step is to extract the axial potential from this configuration and use it to solve (1) with the conditions expected during the focusing experiment. Fig. 4 shows the result of the calculation. This particular beam shape was obtained with a negative potential $V_F = 5.5$ kV. The rest of the required parameters were extracted from the experimental conditions to be presented in the next subsection.

2.3 Experimental Data

The first series of experiments were aimed at estimating the amount of spreading of the charged beam. The results are summarized in Fig. 5, where current density measurements were performed at three different axial positions from the extractor/emitter plane. It is

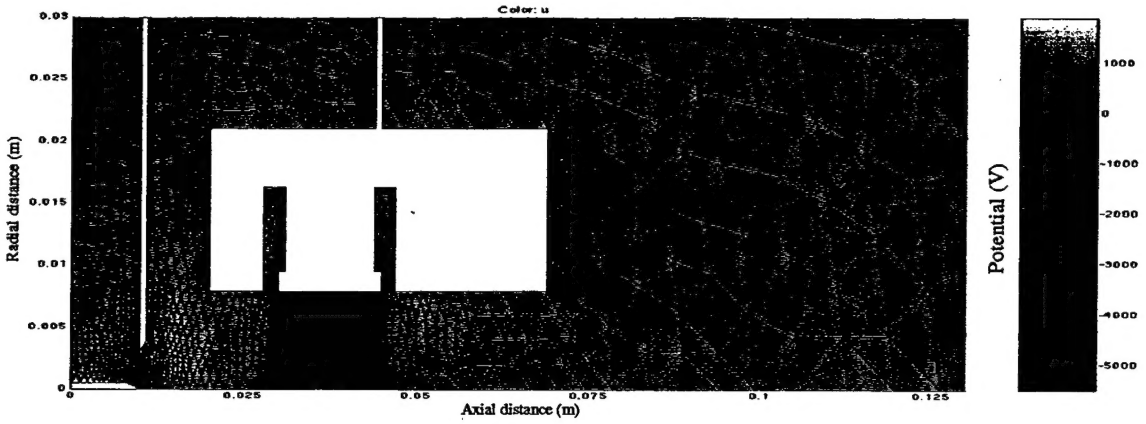

Fig. 3: Computational domain - emitter, extractor and einzel lens

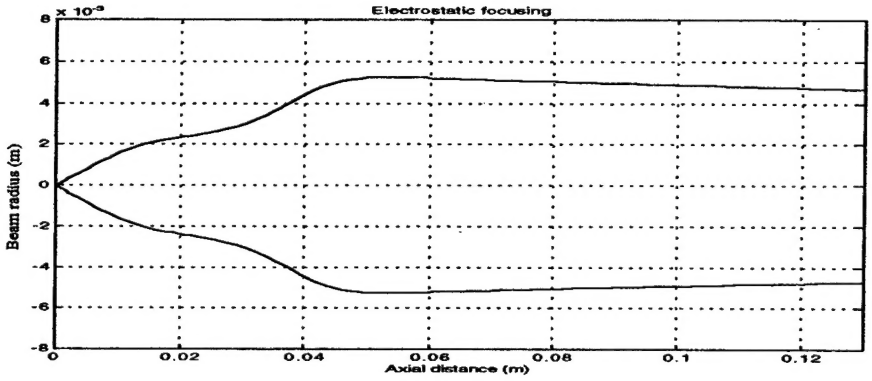

Fig. 4: Trajectory calculation from the paraxial ray equation

interesting to note that for the first two measurements (L = 3.5 and 7 cm) a more or less uniform charge density profile can be observed. For the third measurement (L = 13 cm) the profile is also almost uniform but occupies the whole area of the detector. From the cutoff values of the current and the distances involved, a semi-angle of about 18 ° can be calculated.

In the second experiment, the einzel lens was installed in the system and the current collector was positioned at a distance L=13 cm. Fig 6 shows the current collected by the innermost circle of the detector (r < 0.5 cm) as a function of various negative lens potentials. We observe that a maximum in current (72 nA) is obtained when V_F is around 5.5 kV. This value of current was introduced in the solution of the paraxial ray equation in subsection 2.2. The result of the calculation indicates that a beam "spot" of less than 0.5 cm in radius is generated at the distance where the detector is (Fig. 4.)

In all cases the emitter to extractor potential was held at 1.9 kV. This value was determined at atmospheric pressure by visual inspection of a stable cone at the needle tip and measurement of a stable current.

2.4 Discussion

Experimental results have indicated that focusing is possible for beams of charged particles emitted from colloid thrusters. Nevertheless, more work is required to refine the results presented here. In particular, controllability of the flow rate is important for both the determination of some spray characteristics and for ensuring good experimental repeatability.

Even with such uncertainties, the measurements are well correlated to mathematical modeling. Future work will include a refinement in the measurements presented here, including TOF spectroscopy with the help of electrostatic focusing.

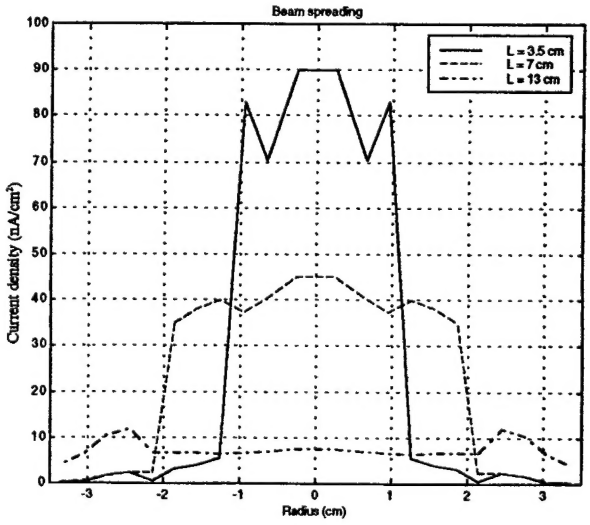

Fig. 5: Current density distributions (experimental)

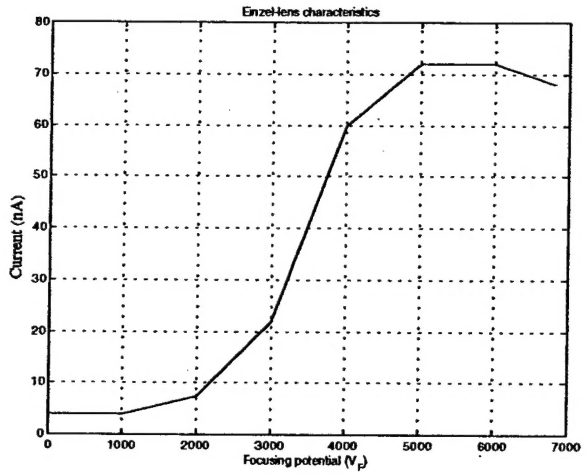

Fig. 6: Electrostatic focusing (experimental)

3. A Dynamic Model of an Emitting Cone-Jet

The structure and performance of the individual emitting cone-jets which underlay colloid thrusters (and, in slightly modified form, field-emission thrusters) has been the object of many studies by electro-spray and ion emission spectroscopy scientists. The seminal work was done by Taylor [5], who first identified the 49.3° cone as the electro-capillary equilibrium shape under idealized conditions. The equilibrium shapes and internal pressures for more general conditions were computed by Pantano and Gañán Calvo [6], who used a boundary element method for the (axisymmetric) electrostatic calculations. They imposed Taylor's angle as a tip boundary condition (in place of the thin jet which actually develops), and were able to determine the cone's volume and existence voltage as a function of size and internal pressure. Gañán Calvo [7] developed an analytical model for the cone-jet combination with a few reasonable simplifications, and obtained scaling laws and definite predictions for jet shape and diameter, surface field distributions and emitted current. Similar, more detailed analytical results were presented by Cherney [7] recently. Both Gañán Calvo's and Cherney's results confirm and explain the semi-empirical laws obtained by Fernandez de la Mora [4] based on extensive experimentation with many conducting fluids.

Our current work is aimed at extending these previous results by constructing a flexible numerical model of the cone-jet combination, which can serve as the basis for assessing a large number of parameters and physical effects. The formulation is axisymmetric, and quasi-one dimensional, but not necessarily steady; solutions are sought by time-marching, which is helpful for understanding the numerical issues, and also yields information on the dynamics of the cone-jet structure. Much of the formulation was initiated by V. Khayms [9], who pursued a steady state solution through direct iteration.

3.1 Formulation

Fig. 7 shows a schematic of a section of the liquid. The volume in an element such as that shaded in the figure, divided by dx, is

$$Vol = \frac{2\pi R^2}{\cos\alpha(1+\cos\alpha)} \tag{3}$$

and the volume flux crossing it is

$$Q_x = \frac{2\pi R^2 u}{1+\cos\alpha} \tag{4}$$

The mass conservation law is then

$$\frac{\partial(Vol)}{\partial t} + \frac{\partial Q_x}{\partial x} = 0 \tag{5}$$

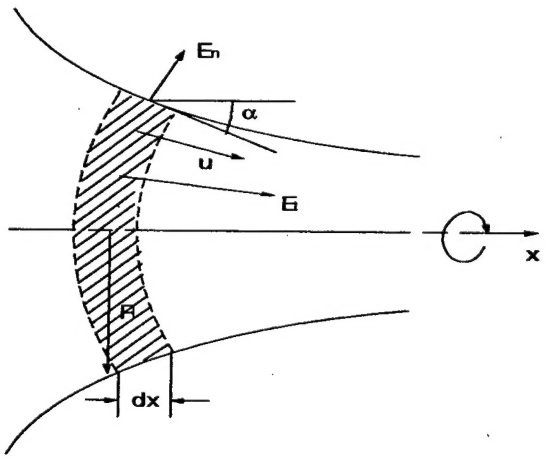

Fig. 7: Modeled Geometry. The shaded volume element is a section of a spherical shell perpendicular to the liquid surface. All quantities are assumed constant on one such shell, and u, E, are assumed perpendicular to its spherical boundaries.

Similarly, the net charge in the element (per unit axial length), is

$$Ch = \frac{2\pi R\sigma_s}{\cos\alpha} \tag{6}$$

where, if the fluid is conductive, $\sigma_s = \varepsilon_o E_n$, E_n being the outside normal electric field. The bulk carries no net charge. The net charge flux, or current, contains two contributions, one from surface charge convection, the other from bulk conduction. The fluid conductivity, K, is treated as a constant, and one obtains

$$I_x = 2\pi\left(uR\sigma_s + \frac{R^2 K E_t}{1+\cos\alpha}\right) \tag{7}$$

Hence, charge conservation requires

$$\frac{\partial (Ch)}{\partial t} + \frac{\partial I_x}{\partial x} = 0 \tag{8}$$

where possible ion emission or electron capture at the surface have been ignored. The x-momentum per unit axial distance is

$$(Mom) = \frac{\rho u \pi R^2}{\cos\alpha} \tag{9}$$

and, including the electrical surface traction $\tau_E = \varepsilon_o E_n E_t$, the axial momentum balance is then

$$\frac{\partial (Mom)}{\partial t} + \frac{\partial}{\partial x}(\pi R^2 \rho u) = -\pi R^2 \frac{dP}{dx} + 2\pi R \varepsilon_0 E_n E_t \tag{10}$$

The final mechanical equation required is a balance of normal forces on a surface element:

$$p + \frac{\varepsilon_0}{2} E_n^2 = \frac{\cos\alpha}{R} - \cos^3\alpha \frac{d^2 R}{dx^2} \qquad (\tan\alpha = -\frac{dR}{dz}) \tag{11}$$

where the two terms on the right are the two principal curvatures of the liquid surface.

The tangential field is related to the surface potential through

$$E_t = -\cos\alpha \frac{d\phi}{dx} \tag{12}$$

The relationship between ϕ and the normal field $E_n = \sigma_s/\varepsilon_o$ is more complex, since every charge in the system (on the liquid as well as on the electrodes) influences each local potential. We use for this a boundary-element method similar to that in Ref.[6]. The contribution $\delta\phi_i$ to the potential at point i, due to the charge on a surface ring at j, with axial extent δx_j is written as

$$\delta\phi_i = N_{ij} (E_n)_j \tag{13}$$

where

$$N_{ij} = \frac{1}{2\pi} \sqrt{m} K(m) \sqrt{\frac{R_j}{R_i}} \frac{\delta x_j}{\cos\alpha_j} \tag{14}$$

and

$$m = \frac{4 R_i R_j}{(x_i - x_j)^2 + (R_i + R_j)^2} \tag{15}$$

and $K(m)$ is the complete elliptic integral of the first kind. In order to simulate a grounded electrode at $x = L$, an "image ring" with an equal and opposite charge is also included. This amounts to replacing $\sqrt{m}K(m)$ by $\sqrt{m}K(m) - \sqrt{m_i}K(m_i)$ in (14), where m_i is as in (15), but with x_j replaced by $2L - x_j$.

The full matrix N_{ij} is then partitioned into blocks representing potential on liquid points due to charges on liquid elements ($N_{\ell\ell}$), potential at liquid points due to charges on the metal supply tube ($N_{\ell t}$), etc. We then have the matrix equations

$$\phi^\ell = N_{\ell\ell} E_n^{\ell} + N_{\ell t} E_n^{t} \tag{16}$$

$$\phi^t = N_{t\ell} E_n^{\ell} + N_{tt} E_n^{t} \tag{17}$$

where E^ℓ, E^t are numerical vectors collecting all normal fields on the liquid and on the tube, respectively. Imposing a known tube potential V, and eliminating E^t between (16) and (17) leads to

$$\phi^\ell = N_{\ell t} N_{tt}^{-1} V + (N_{\ell\ell} - N_{\ell t} N_{tt}^{-1} N_{t\ell}) E_n^{\ell} \tag{18}$$

which is the desired (global) relationship between normal fields and potentials on the liquid surface. The numerically intensive matrix inversion N_{tt}^{-1} needs to be done only once for a given geometry, but the matrices $N_{\ell t}, N_{\ell\ell}, N_{t\ell}$ have to be updated as the liquid shape evolves.

3.2 Numerical Implementation

A fixed 1-D grid is generated, with highest resolution near the expected cone tip and near the tube mouth, where a field singularity is expected due to the sharp change of surface slope. For initialization of variables, as well as for selection of appropriate grid spacing, the dimensionless results of Ref [7] have been used. Spatial derivatives are approximated to 2nd order on the uneven grid, and a first-order Euler step is used for temporal updating of (*Vol*), (*Ch*) and (*Mom*), using Eqs. (5), (8) and (10), respectively. After the updates, the primary variables (R, α, u, E_n) are extracted from the updated quantities, p is calculated from (11), and Eq. (18) is used to calculate the new potential distribution. E_t then follows from (12), and a new updating cycle can begin.

The time step Δt used for updating needs to be smaller than both, the charge relaxation time $\tau_{Rel} = \varepsilon_0 / K$ and the smallest passage time through one grid cell, $\tau_{Res} = (\Delta x_i / u_i)_{\min}$. For liquids of high conductivity, ($K >$ 1 Si/m), τ_{Rel} is less than about 10^{-11} s, well below τ_{Res}, and short enough that complete simulation through a few microseconds may be impractical. For these situations, a modified procedure is necessary, in which the cone region is assumed electrically (not mechanically) relaxed all the time (i.e. $I_x(x,t) = I(t)$), but the jet region current is allowed to evolve dynamically. The level of current $I(t)$ is then determined by the value of I_x at the cone-jet transition. This has not yet been implemented. Instead, work has concentrated

on cases with lower conductivity ($K \leq 0.01$ Si/m), for which an extensive data base exists Refs. [2,3].

3.4 Jet Instability and Spray Dynamics

Even in the absence of charge, the jet would pinch itself into droplets at some downstream distance, following growth of the Rayleigh-Taylor instability. The presence of charge can only accentuate this tendency. For purely convected surface charges, a linearized stability analysis presented in Ref.[10] obtained the dispersion relation

$$\omega^2 = -\frac{\gamma}{\rho R_0^3}\frac{xI_1(x)}{I_0(x)}\left\{1 - x^2 + F_c\left[\frac{xI_0(x)}{I_1(x)} - 1\right]\right\} \qquad (19)$$

where γ is the surface tension, R_0 is the local mean radius, $x = kR_0$, k being the wavenumber, I_0 and I_1 are modified Bessel functions, and

$$F_c = \frac{\rho^2 R_0^3}{4\varepsilon_0 \gamma}\left(\frac{q}{m}\right)^2 \qquad (20)$$

is a measure of the state of charge, which is of order unity in electrospray jets. Negative values of ω^2 imply the existence of an exponential growth mode. Eq. (19) is plotted in Fig. 8. The case $F_c = 0$ is the classical result of Rayleigh and Taylor, with peak growth at $x \cong 0.7$, leading to an eventual radius of the pinched droplets $R_D \cong 1.89 R_{Jet}$. For $F_c \sim 1$, somewhat smaller droplets are indicated ($R_D \cong 1.6 - 1.7 R_{Jet}$), but also faster growth of the instability. Also of interest for our simulation, all wavelengths are seen to be unstable, although only weakly so for the longer ones (small x).

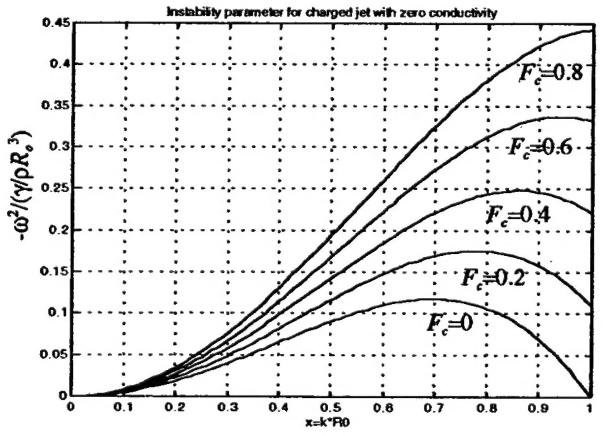

Fig. 8: Dispersion relation

In the jet simulation, the axial grid spacing Δx is of the order of the jet radius at the neck, although it is later allowed to grow much larger. It is therefore possible to capture the growth of the jet instability and the jet pinching near the neck. Fig. 9 shows an example, corresponding to a Formamide cone-jet with K=0.01 Si/m, $Q = 7.84 \times 10^{-12}$ m^3/s, V=2000V. The time after simulation start is $t = 5.5 \times 10^{-7}$s, and $x = 1.2 \times 10^{-5}$m corresponds to about 3-4 jet diameters downstream of the cone's neck.

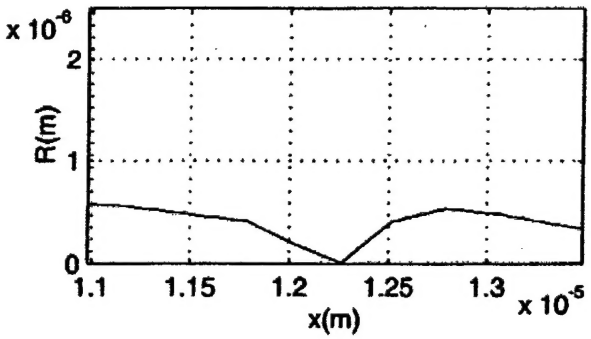

Fig. 9: Numerical prediction of jet pinching

Using γ= 0.05N/m, ρ = 1130kg/m^3, and (from Fig. 8) a maximum normalized ($-\omega^2$) of 0.5, the exponential time constant for growth is predicted to be $7 \times 10^{-8} s$, and the most unstable wavelength to be 3μm. Fig. 9 shows pinching in about 8 time constants (a reasonable result), and roughly confirms the 3μm wavelength.

A detailed computation of the jet breakup process is however, beyond the scope of this quasi-one-D model. In order to continue capturing the electrostatic effect of the jet on the cone, we need to replace the jet equations by a set of "spray" equations beyond the breakup point. For this, a time-dependent variation of the Paraxial Ray method will be used, although this is yet to be implemented. The spray flux is assumed uniform up its edge (consistent with our experimental results elsewhere in this paper), and the expansion yields a radial field at r=R of

$$E_n = \frac{R}{2}\frac{\partial^2 \phi}{\partial x^2} + \frac{M}{(q/m)2\pi R\varepsilon_o} \qquad (21)$$

where M is the mass contained in unit length of the spray (and it obeys a conservation equation $\frac{\partial M}{\partial t} + \frac{\partial (Mu)}{\partial x} = 0$), and q/m is the locked-in charge-to-mass ratio, carried over from the jet. The velocity components u(axial) and v(radial) obey

$$\frac{\partial u}{\partial t} + u\frac{\partial u}{\partial x} = \frac{q}{m}E_t \qquad (22)$$

$$\frac{\partial v}{\partial t} + u\frac{\partial v}{\partial x} = \frac{q}{m}E_n \qquad (23)$$

and the spray radius then evolves according to

$$\frac{\partial R}{\partial t} + u\frac{\partial R}{\partial x} = v \qquad (24)$$

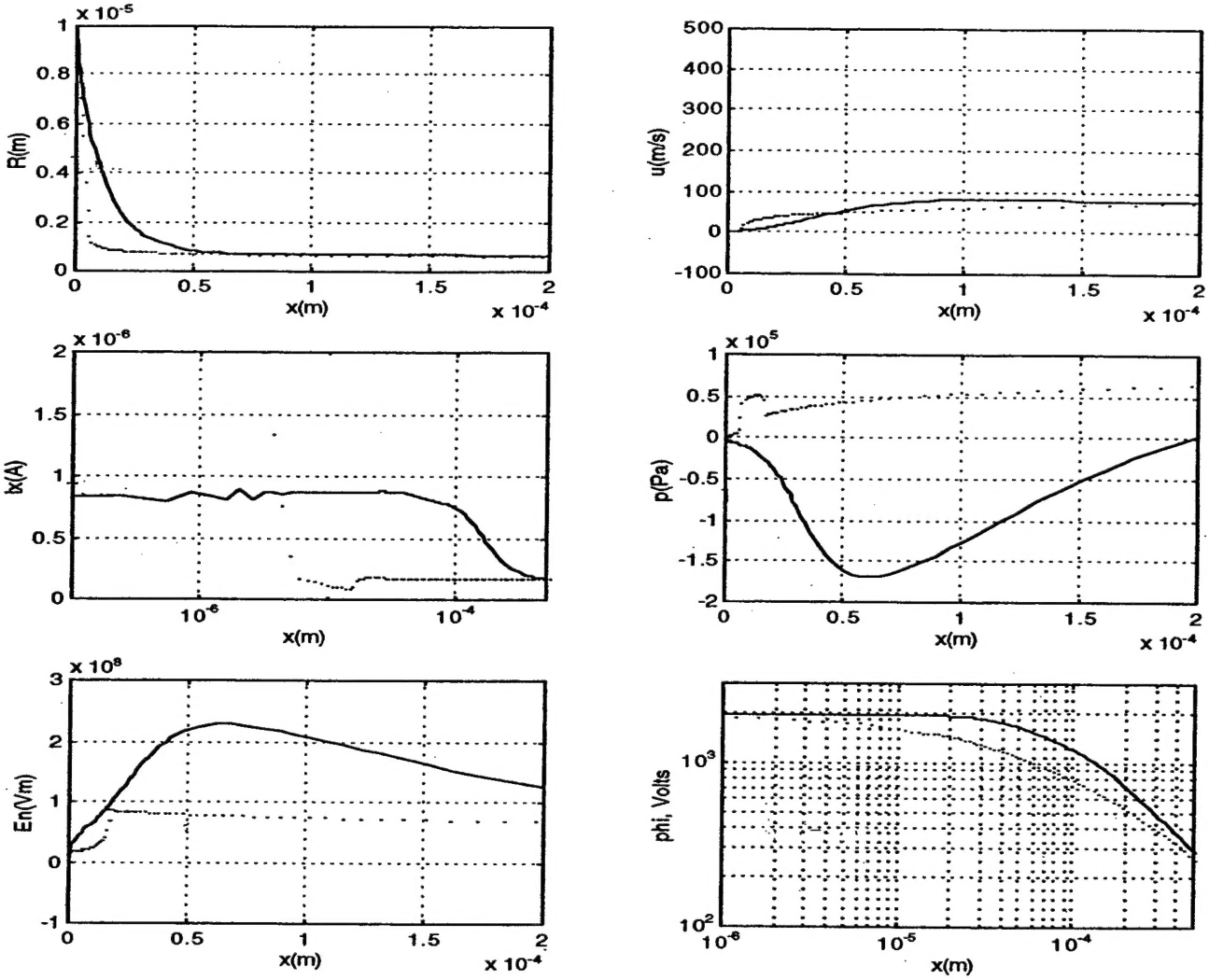

Fig. 10: Preliminary numerical results. Dotted line, $t = 0$.
Continuous line, $t = 1.3$ μs

With some uncertainty, arising from the details of the breakup process, these equations will allow computation of the spread of non-neutralized electrospray plumes, and will find use in the design and analysis of TOF experiments, as planned in our laboratory.

3.5 Some Preliminary Results

Fig. 10 shows a sample of results pertaining to a cone-jet of Formamide, with a conductivity K=0.001Si/m, at a flow rate Q=7.84×10^{-11} m^3/s, which is a few times the minimum stable flow for that conductivity [4]. This conductivity level is also what can be obtained in concentrated Glycerol solutions, as in the first generation of colloid thrusters [1]. The delivery tube, at V=2000Volt, has a radius of 10 μm with a sharp, chamfered lip, and is assumed placed 1mm away from a grounded collector plane. Shown are profiles of liquid radius R, velocity u, local current I_x, pressure p, normal electric field E_n, and potential ϕ. For each of these, we show the initial profiles assumed, and those computed after about $1.3\times10^{-6}s$. This time is about 1/8 what it would take to "fill" a Taylor cone of the assumed size, at the assumed flow rate, so that convergence is still incomplete. The time step used was $2\times10^{-11}s$, about 1/500 of the fluid's relaxation time; increasing this to $2\times10^{-10}s$ resulted in strong numerical oscillations near the tube exit.

Several observation can be made: Firstly, at 1.3 μs, the local current I_x has relaxed to a near-constant value of 8×10^{-7}A, several times higher than the expected steady-state value, based on the empirical data of [4], which was used in the initialization (and is visible in the parts of the jet not yet affected). This level exhibits a slow decay rate over time, as the extent of the relaxed zone spreads forward. It should be noted that the

flattening of the I_x profile was already evident at times of the order of $1\times10^{-8}s$, i.e., the relaxation time at the chosen conductivity.

The peak normal field is about 0.2-0.3 V/nm, and occurs near the front of the spreading relaxation zone. Because of its high value, the liquid pressure is seen to change from its initial distribution (near zero in the cone, positive in the jet) to between 1 and 2 atm. negative. This might imply liquid breakup, although metastability may hold it together during this transient. The potential is nearly constant in the cone, falling by some 200 Volt near the tip, and more rapidly beyond it. The cone itself has been elongating, from some 9 μm initially (following the assumed Taylor angle), to some 20 μm at the 1.3 μs time point.

We note finally that the jet has not yet shown signs of pinching in this simulation, whereas for K=0.01 Si/m, pinching was shown (Fig. 9) at about 0.5 μs. This is to be expected from the $R^{3/2}$ dependence of the instability growth time (Eq. 19), and the variation of R at minimum flow as $K^{-2/3}$ (Ref. 4).

4. Conclusions

The ability to reverse the electrostatic spreading of a non-neutralized colloidal jet has been experimentally demonstrated, which opens the way for improved diagnostic instrumentation. A new method for numerical simulation of the cone-jet dynamics has been developed, and preliminary results are encouraging.

References

1. M. Martinez-Sanchez, J. Fernandez de la Mora, V. Hruby, M. Gamero-Castaño and V. Khayms, "Research on Colloid Thrusters". Paper IEPC 99-014, 26th International Electric Propulsion Conference, Kitakyushu, Japan, Oct. 1999.
2. M. Gamero and V. Hruby, "Electrospray as a source of nanoparticles for efficient colloid thrusters", paper AIAA-2000-3265, 36th Joint Propulsion Conference, Huntsville, AL, July 2000.
3. J.W. Ward, R.L. Seigler, "Trajectory calculations of liquid metal ion sources", J. Vac. Sci. Technol., 19(4), Nov/Dec 1981, p. 1082
4. J. Fernandez de la Mora and J.G. Loscertales, "The current emitted by highly conducting Taylor cones". J. Fluid Mech., vol 260, pp 155-184 (1994)
5. G.I Taylor, "Disintegration of water drops in an electric field", Proc. R. Soc. London, A 280, 383-397.
6. C. Pantano, A.M. Gañán-Calvo and A. Barrero, "Zeroth-order electrostatic solution for electrospraying in Cone-Jet mode" J. Aerosol Sc., V. 25, N. 6, 1065-1077 (1994).
7. A. Gañán-Calvo, "Cone-Jet analytical extension of Taylor's electrostatic solution and the asymptotic universal scaling laws in electrospraying" Phys. Rev. Let., V. 79, N. 2, july 1997.
8. L. Cherney, "Structure of Taylor cone-jets: limit of low flow rates". J. of Fluid Mech., (1999). V. 378, pp 167-196.
9. V. Khayms, "Advanced Propulsion for Micro-satellites", Doctoral Thesis, MIT, Sept. 2000.
10. M. Martinez-Sanchez, et.al., in the Interim Progress Report on NASA SBIR 16.01, May 2000.